Molecular Therapy
Methods & Clinical Development
Original Article

7T MRI Predicts Amelioration of Neurodegeneration in the Brain after AAV Gene Therapy

Heather L. Gray-Edwards,[1] Anne S. Maguire,[1,2] Nouha Salibi,[3] Lauren E. Ellis,[1] Taylor L. Voss,[2] Elise B. Diffie,[1,2] Jey Koehler,[4] Ashley N. Randle,[1] Amanda R. Taylor,[5] Brandon L. Brunson,[2] Thomas S. Denney,[6,7] Ronald J. Beyers,[6] Atoska S. Gentry,[1] Amanda L. Gross,[1,2] Ana R. Batista,[8] Miguel Sena-Esteves,[8] and Douglas R. Martin[1,2]

[1]Scott-Ritchey Research Center, College of Veterinary Medicine, Auburn University, Auburn, AL, USA; [2]Department of Anatomy, Physiology and Pharmacology, College of Veterinary Medicine, Auburn University, Auburn, AL, USA; [3]MR R&D Department, Siemens Healthcare, Malvern, PA, USA; [4]Department of Pathobiology, College of Veterinary Medicine, Auburn University, Auburn, AL, USA; [5]Department of Clinical Sciences, College of Veterinary Medicine, Auburn University, Auburn, AL, USA; [6]MRI Research Center, Auburn University, Auburn, AL, USA; [7]Department of Electrical Engineering, Auburn University, Auburn, AL, USA; [8]Department of Neurology, University of Massachusetts Medical School, Worcester, MA, USA

GM1 gangliosidosis (GM1) is a fatal neurodegenerative lysosomal storage disease that occurs most commonly in young children, with no effective treatment available. Long-term follow-up of GM1 cats treated by bilateral thalamic and deep cerebellar nuclei (DCN) injection of adeno-associated virus (AAV)-mediated gene therapy has increased lifespan to 8 years of age, compared with an untreated lifespan of ~8 months. Due to risks associated with cerebellar injection in humans, the lateral ventricle was tested as a replacement route to deliver an AAVrh8 vector expressing feline β-galactosidase (β-gal), the defective enzyme in GM1. Treatment via the thalamus and lateral ventricle corrected storage, myelination, astrogliosis, and neuronal morphology in areas where β-gal was effectively delivered. Oligodendrocyte number increased, but only in areas where myelination was corrected. Reduced AAV and β-gal distribution were noted in the cerebellum with subsequent increases in storage, demyelination, astrogliosis, and neuronal degeneration. These postmortem findings were correlated with endpoint MRI and magnetic resonance spectroscopy (MRS). Compared with the moderate dose with which most cats were treated, a higher AAV dose produced superior survival, currently 6.5 years. Thus, MRI and MRS can predict therapeutic efficacy of AAV gene therapy and non-invasively monitor cellular events within the GM1 brain.

INTRODUCTION

GM1 gangliosidosis (GM1) is a fatal lysosomal storage disorder caused by mutations in the *GLB1* gene encoding the lysosomal enzyme, β-galactosidase (β-gal; EC 3.2.1.23). GM1 affects individuals of all ages and can be clinically classified into four categories: infantile, late infantile, juvenile, and adult onset.[1] Subtype classification is largely based on age of onset and disease severity, and often correlates with residual β-gal activity associated with a given mutation. All subtypes result in storage of GM1 ganglioside and its asialo derivative (GA1) throughout the central nervous system, predominantly within neurons, with storage rate proportional to disease severity.[2] Ganglioside storage is accompanied by classical neurodegenerative mechanisms, including astrogliosis, microgliosis, demyelination, and neuroaxonal degeneration.[2–4] Although each of these neurodegenerative mechanisms is known to occur in GM1, their timing relative to disease onset and severity remains unknown. Although difficult to do in humans, clinical and histopathologic correlates in GM1 animals over time can further define the relationship between disease progression and cellular change within the brain. Once established, these clinical biomarkers can be used to determine whether neurodegenerative features are ameliorated by novel therapeutics.

Magnetic resonance spectroscopy (MRS) provides detailed biochemical information on toxic metabolites, neuronal degeneration, demyelination/dysmyelinogenesis, and changes in cell populations.[5–7] Levels of other normal brain metabolites can provide insight into the biochemical changes that occur during GM1. Impaired neuronal function, injury, and death can be monitored directly through the measurement of *N*-acetylaspartate (NAA), a marker of neuroaxonal integrity.[8,9] Demyelination and/or dysmyelinogenesis, other pathological hallmarks in patients with GM1,[10–14] can also be quantified by measuring choline (Cho), which primarily consists of the cell membrane components phosphocholine and glycerophosphocholine.[8,15] Demyelination can be further monitored as smaller breakdown products detected lower in the spectra in the form of lipid peaks.[6] Gliosis is also a histopathologic finding because GM1 gangliosides accumulate within glial cells, resulting in their activation and proliferation.[10,16,17] Gliosis can be directly

Received 6 August 2019; accepted 13 November 2019;
https://doi.org/10.1016/j.omtm.2019.11.023.

Correspondence: Douglas R. Martin, 245 Scott-Ritchey Research Center, 1265 HC Morgan Drive, College of Veterinary Medicine, Auburn University, AL 36849, USA.
E-mail: martidr@auburn.edu

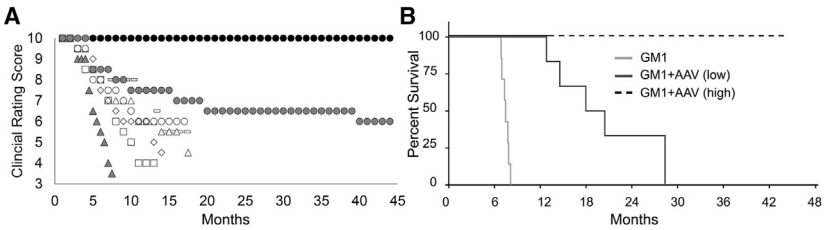

Figure 1. Clinical Disease Progression and Survival of GM1+AAV-Treated Cats

(A) Clinical rating scores representing neurologic disease in normal cats (black circles), a representative untreated GM1 cat (closed gray triangles), a GM1 cat treated with AAV at a high dose (closed gray circles), and GM1 cats treated with AAV at a low dose (open symbols). (B) Kaplan-Meier survival curve. GM1 cat treated with AAV at a high dose (black line), GM1+AAV low-dose cats (dark gray line), and untreated GM1 cats (light gray line).

monitored using MRS to measure myoinositol (Ins), a marker of glial cell number.[6,15,18]

Feline GM1 faithfully recapitulates late-infantile GM1. First reported in the 1970s, the feline GM1 model has been meticulously studied and exhibits a similar phenotype, lipid storage profile, and ganglioside metabolism[19,20] compared with humans. Body fluid and MRI-based biomarkers also correlate between GM1 cats and human patients.[21] Thus, the feline model has many advantages for testing long-term efficacy of novel therapeutics. We developed an adeno-associated virus (AAV)-mediated gene therapy that exhibits extraordinary efficacy in GM1 mice and cats,[22–24] with an average survival increase >7.5-fold after gene therapy.[20] Currently, two of the treated cats from the original report[20] remain healthy, with only mild disease at >8 years of age (untreated lifespan of 8.0 ± 0.6 months).

The unprecedented success of gene therapy in the GM1 animals has led to consideration of human clinical trials. Although efficacious, the previously reported route of administration (combined thalamic [Thal] and cerebellar injection) is generally cautioned against in humans due to the surgical risk for cerebellar hemorrhage and brainstem herniation from increased pressure in the posterior fossa. In our previous studies in cats,[20,21,25,26] we rarely encountered excessive hemorrhage from the cerebellar injection sites. However, the cat cerebellum is positioned caudal to the cerebrum and is more easily approached than the human cerebellum, located ventral to the cerebrum. In an attempt to minimize risk in children, we tested intracerebroventricular (i.c.v.) injection as an alternative delivery route to the cerebellum via cerebrospinal fluid (CSF). Post mortem analyses were performed at multiple time points in untreated GM1 cats and in GM1 cats treated with gene therapy to evaluate: (1) therapeutic efficacy and (2) ultra-high-field (7-tesla [7T]) MRI and MRS as non-invasive objective measures for future clinical trials. Direct measurement of brain biochemistry by MRS in the feline GM1 brain strongly correlates with disease progression, facilitating non-invasive assessment of the effects of intracranial gene therapy for GM1 and providing a framework for future human clinical trials.

RESULTS

To evaluate efficacy in a reasonable time frame, we treated most cats in the current study by a reduced dose relative to the original report, in which treated GM1 cats survived many years.[20,21] GM1 cats underwent i.c.v. and bilateral Thal injection of an AAVrh8 vector encoding feline β-gal at a total dose of 2×10^{12} vg (n = 5) or 5.4×10^{12} vg (n = 1). The cat treated with the high dose remains alive at 6.5 years, whereas those treated with the low dose had a mean survival time of 18.8 ± 6.0 months ($p = 0.014$) compared with the untreated lifespan of 8.0 ± 0.6 months (Figure 1B). In addition to extending lifespan by 2.4- or 8.7-fold in cats treated with the low or high doses, respectively, this therapy clearly improved quality of life and ameliorated disease signs as reflected by a clinical rating scale (Figure 1A). The numerical clinical rating scale was established to measure neuromuscular disease progression in untreated GM1 cats and is described in the Materials and Methods. Three additional GM1 cats treated with the low dose were euthanized at a predetermined time point equivalent to the humane endpoint of untreated GM1 cats (~8 months) for histopathologic and biochemical assessments. Animals euthanized at the predetermined time point were not included in the survival curve.

MRI and MRS

Ultra-high-field (7T) MRI and MRS were performed on untreated GM1 cats at 4 months and at the humane endpoint (~8 months). AAV-treated GM1 cats were divided into short-term (~8 months) and long-term cohorts (humane endpoint) and underwent MRI at both time points. On T2-weighted (T2W) MRI, macroscopic GM1 storage in gray matter is visualized as a darkening (hypointensity), whereas demyelination of white matter is represented by a lightening (hyperintensity) (Figure 2A). These two pathologic events result in the brain taking on an overall gray appearance and reduction of contrast between gray and white matter (isointensity).[10,27] In the untreated GM1 cerebrum and cerebellum at 8 months, the gray and white matter were isointense compared with the normal cat.[10,27] After gene therapy, intensity changes were largely ameliorated throughout the brain with the exception of the temporal lobe (white box) and portions of the cerebellum. T2W MRI images, like those depicted in Figure 2A, were quantitated as percent of low lipid signal (light-gray), high lipid signal (dark gray), and aqueous signal (white, CSF; Figures 2B–2E). In general, untreated GM1 cat brains had an increased percentage of high lipid signal, which replicates findings in human GM1 patient MRIs and is consistent with ganglioside storage in cell bodies.[28] Quantitation of MRIs in GM1+AAV cats corroborated anatomical assessments that brain architecture was largely preserved by gene therapy.

MRS was utilized to quantify levels of metabolites that represent gliosis, demyelination, and neuro-axonal loss in feline GM1. Six voxels of the brain were analyzed, with emphasis on the cerebellum (Figure 3) because treatment of the cerebellum without parenchymal injections

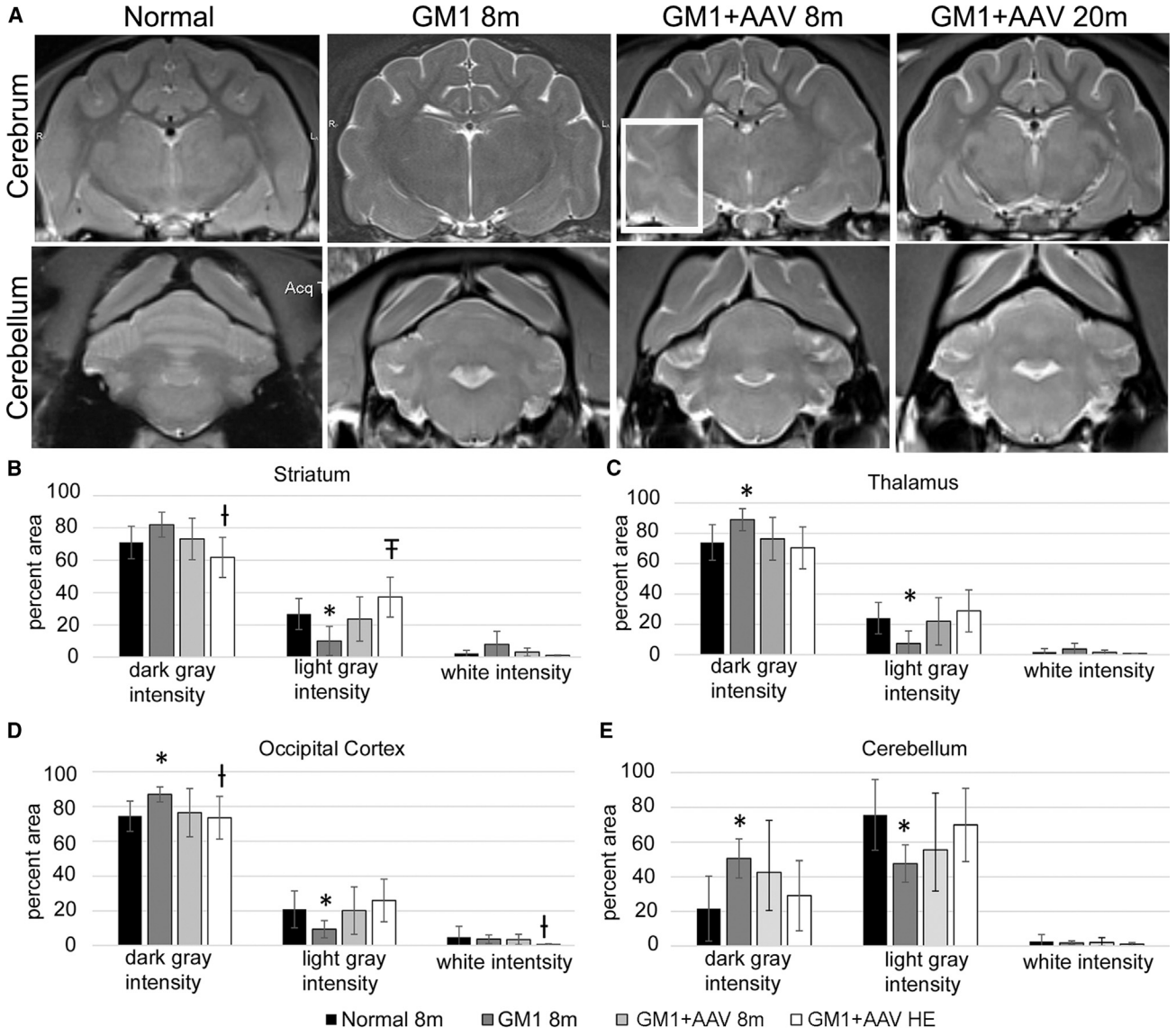

Figure 2. 7T MRI of GM1 Cats after Gene Therapy

(A) In T2-weighted images from normal cats, white matter is represented by dark gray regions and gray matter by light gray regions. CSF is represented by white pixels. In the GM1 cat, there is an overall isointensity or lack of difference between the gray and white matter in the cerebral cortex and cerebellum. At 8 months in the AAV-treated cats (low dose), the brain is largely normalized except for the temporal lobe (white box) and parts of the cerebellum. (B–E) Intensities on MRI were calculated in an individual slice at the level of the striatum (B), thalamus (C), occipital cortex (D), and cerebellum (E) in normal cats, untreated GM1 cats, and low-dose GM1+AAV cats at 8 months and at the humane endpoint. The intensity associated with increased lipid content (dark gray) was increased in GM1 untreated cats because of ganglioside storage in cell bodies of the gray matter. After treatment, gray and white matter intensities are normalized. *$p < 0.05$, **$p < 0.01$ from age-matched normal cats; $^{\dagger}p < 0.05$, $^{\mp}p < 0.01$ from untreated GM1 cats at the humane endpoint. Error bars represent standard deviation.

is a focus of this study. By 4 months of age there was a reduction in the neuroaxonal marker NAA and an increase in the markers of demyelination, glycerophosphocholine and phosphocholine (GPC+PCh). By the humane endpoint, the GM1 cat exhibited more pronounced reduction of NAA and a reduction of NAA+*N*-acetyl aspartyl glutamate (NAAG), also a marker of neuronal health. GPC+PCh increased further at the humane endpoint, and an increase in markers of gliosis (Ins) and metabolism (creatine and phosphocreatine [Cr+PCr]) was noted. The untreated GM1 cat at humane endpoint also exhibited a decrease of the neurotransmitters glutamate and glutamine (Glu+Gln). With the exception of Ins at the 8-month time point, low-dose AAV gene therapy failed to correct any of these alterations in the cerebellum of GM1 cats. High-dose gene therapy (n = 1, ongoing) has thus far resulted in increased survival to 6.5 years,

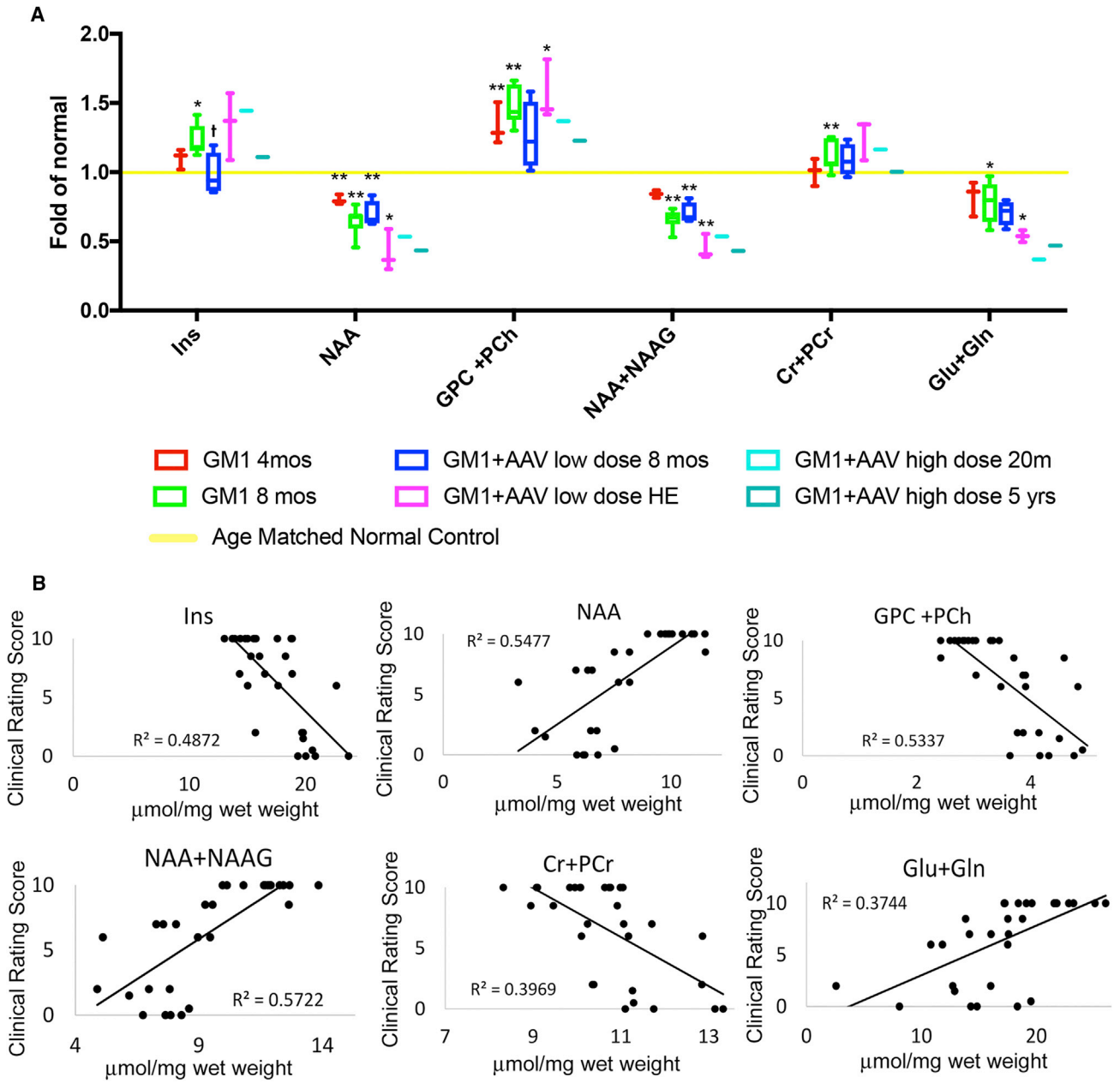

Figure 3. MRS of the Cerebellum after AAV Gene Therapy

Brain metabolites were measured in untreated GM1 cats at early disease stage (4 months) and humane endpoint (~8 months), and in age-matched normal controls (yellow line). Also measured were GM1+AAV-treated cats at 8 months or long term. The following metabolites were included: myoinositol (Ins, a marker of gliosis), *N*-acetylaspartate (NAA, a marker of neuroaxonal health), glycerophosphocholine and phosphocholine (GPC+PCh, an indication of demyelination), NAA+*N*-acetyl aspartyl glutamate (NAAG, also indicating neuroaxonal health), creatine and phosphocreatine (Cr+PCr, markers of metabolism), and glutamate and glutamine (Glu+Gln, markers of the glutaminergic neurotransmitter recycling system). (A) Partially or fully corrected metabolites of GM1 cats treated by gene therapy included Ins, GPC+PCh, and Cr+PCr. *$p < 0.05$, **$p < 0.01$ versus age-matched normal; †$p < 0.05$, ₸$p < 0.01$ from untreated GM1 cats at the humane endpoint. (B) Metabolites were plotted against clinical status (clinical rating scores) at the time of MRS to evaluate correlation with clinical disease (R^2). Error bars represent standard deviation.

with full or partial correction of Ins, GPC+PCh, and Cr+PCr. Metabolites that remained abnormal in the animal treated with the high dose include NAA, NAA+NAAG, and Glu+Gln. In fact, levels of these metabolites approximate those of the low-dose cohort at the humane endpoint. To determine each metabolite's predictive ability, we correlated individual metabolite concentrations from the cerebellum

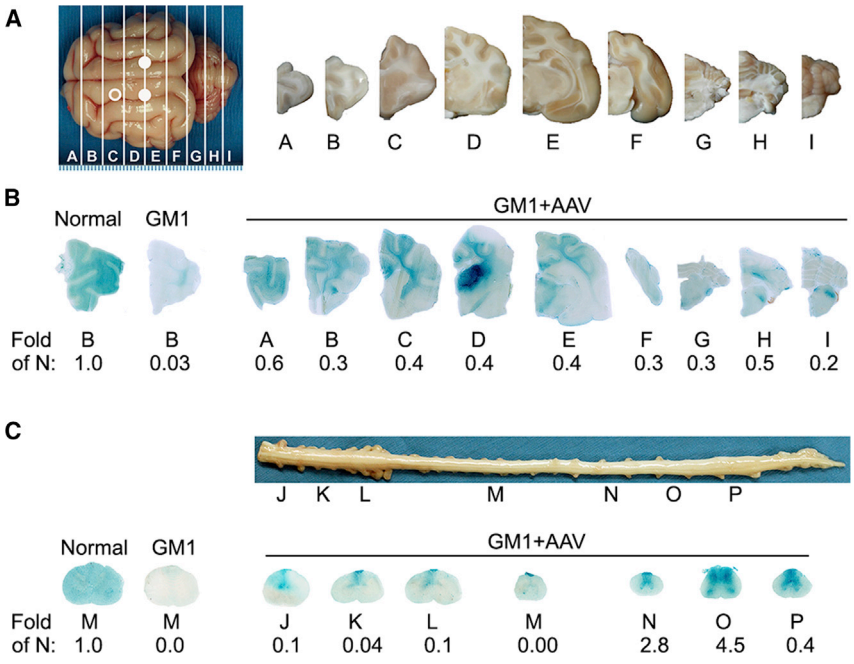

Figure 4. Biodistribution of β-Gal in the Brain and Spinal Cord of GM1+AAV (Low-Dose) Cats

(A) Solid white dots indicate thalamic injection sites, whereas the open white dot represents the lateral ventricular injection site. Cat brain was divided at necropsy into 6-mm blocks, shown by white lines, and blocks were labeled A–I. The right hemisphere was used for β-gal staining and activity assays. (B) Blue histochemical staining represents β-gal activity throughout the brain. Below each stained section is shown quantitative β-gal activity expressed as fold of normal levels. (C) Spinal cord blocks are denoted by letters J–P and correspond to the coronal sections stained for β-gal activity (blue). Shown is a representative example of a GM1 cat treated with the low dose and followed to the humane endpoint (8-1701), as well as control sections from untreated normal and GM1 cats.

with individual clinical rating scores at the time of MRI/MRS. NAA+NAAG, NAA, and GPC+PCh had the greatest correlations, with R^2 values of 0.57, 0.55, and 0.53, respectively.

Metabolite concentrations in the internal capsule, thalamus, parietal cortex, temporal lobe, and occipital cortex were also quantified (Figure S1). Ins was increased in the GM1 cat at humane endpoint in the thalamus and internal capsule, indicating pronounced gliosis. NAA was reduced or trended toward a reduction in all untreated brain areas at both time points, and GPC+PCh was increased in all untreated GM1 voxels at 8 months. In general, low-dose gene therapy resulted in transient, partial correction of a few metabolites, but no persistent correction was measured for any metabolite in any region of the brain with the exception of GPC+PCh in the internal capsule. Partial or full correction of metabolite levels across the brain was most clear in the single cat treated with the high dose, which had near-normal or normal levels of all metabolites in the internal capsule and parietal cortex. Although no single treatment restored all metabolite levels in the thalamus and occipital cortex, the highest degree of normalization was found in the animal treated with the high dose.

Biodistribution

Qualitative biodistribution assays detected β-gal activity throughout the brain, with the highest levels at the injection sites tapering to lower levels elsewhere (blue staining in Figure 4B). When quantitated with a fluorogenic substrate, β-gal activity in the brain ranged from 0.2- to 0.6-fold normal (or 20%–60% normal), which exceeded the hypothesized therapeutic threshold of ~10% normal for most lysosomal enzymes.[1,29,30] Similarly, β-gal activity was detected throughout the spinal cord in seven tested blocks that encompassed the cervical, thoracic, and lumbar regions. Activity was lowest in the cervical and thoracic spinal cord (0.0- to 0.1-fold normal) but reached as high as 4.5-fold of normal in the lumbar region (Figure 4B). Vector biodistribution followed a similar profile, with the greatest amount of vector genomes near the Thal injection site with decreases by two orders of magnitude throughout the remainder of the brain and spinal cord (Table S1).

Storage Clearance

Biodistribution of β-gal inversely correlated with storage material as assessed by periodic acid-Schiff (PAS) staining (converted to grayscale), which was utilized to assess storage clearance after AAV gene therapy (Figure 5). In the GM1 cat, white matter stains lighter and gray matter stains darker than the normal cat due to myelin loss and ganglioside storage, respectively. PAS staining was largely normalized throughout the brain of the AAV-treated cat at both 8 months and the humane endpoint, with the exception of aspects of the temporal and parietal lobes, occipital cortex, and cerebellum. Intensity alterations observed in MRI (i.e., darkening of gray matter and lightening of white matter; Figure 2) showed similar anatomical distribution as the PAS-positive storage material.

Neuroinflammation

To determine whether the neuroinflammatory response was altered by gene therapy, we performed immunohistochemistry for astrocytes (glial fibrillary acidic protein [GFAP]) and microglia (Iba-1). Astrocyte number increased and cells adopted a reactive morphology in the GM1 cat compared with normal (Figure 6A). At 8 months of age (~6 months post treatment), the morphology more closely resembled normal cats, with moderate progression at the humane endpoint in several brain areas including the parietal cortex (Figure 6A). The total area of GFAP staining increased in all brain areas of the GM1 cat (Figure 6B). In treated GM1 cats at 8 months of age, GFAP staining decreased in all areas of the brain except the striatum. However, GFAP staining began to increase again by the humane endpoint, so reductions at the 8-month time point were not permanent

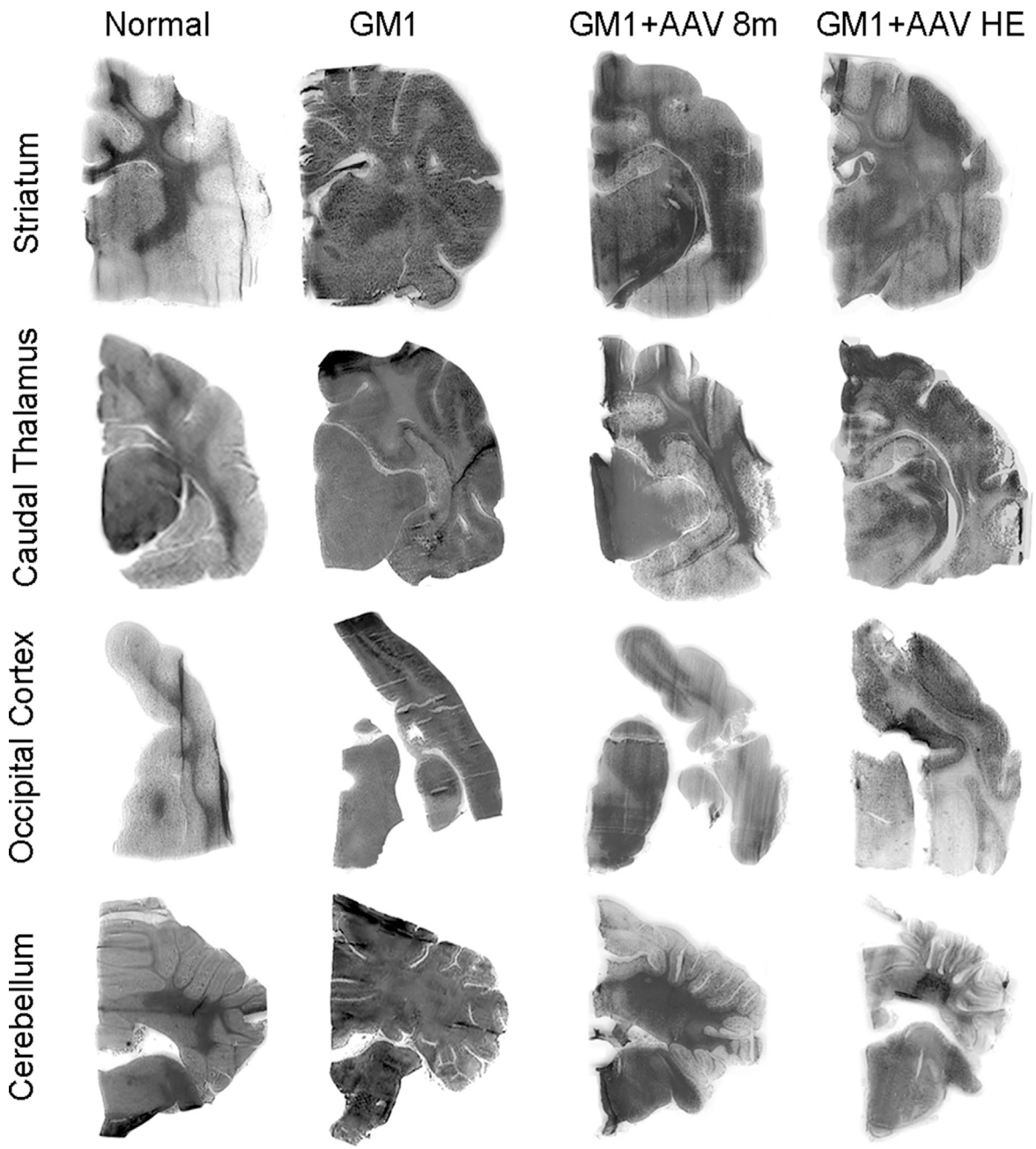

Figure 5. Storage Material in GM1 Cats Treated with the Low Dose of Gene Therapy

Periodic acid-Schiff stain (converted to grayscale) is shown to illustrate the storage pattern in the striatum/parietal cortex, caudal thalamus/temporal cortex, occipital cortex/midbrain, and cerebellum/brainstem. In the normal cat, white matter is darker than gray matter, and this is inverted in the GM1 cat because of high storage levels in neuronal cell bodies. Gene therapy normalized storage levels except in discrete areas of the parietal cortex, temporal lobe, and cerebellum.

(Figure 6B). GFAP staining in the cerebellum mildly correlated with Ins concentration as determined by MRS (R^2 = 0.33; Figure 6C), but highly correlated with the clinical rating score of cats at the time of MRI (R^2 = 0.70; Figure 6D). As estimated by Iba-1 staining, microgliosis was also increased in the untreated GM1 cat. Iba1 staining was intermediate in GM1 cats after gene therapy, although precise quantitation was not possible due to variability in background staining (Figure S2).

Neuronal Degeneration

Degenerative change was widespread in both neuron cell bodies and axons in untreated GM1 cats (Figure S3). Six months after gene

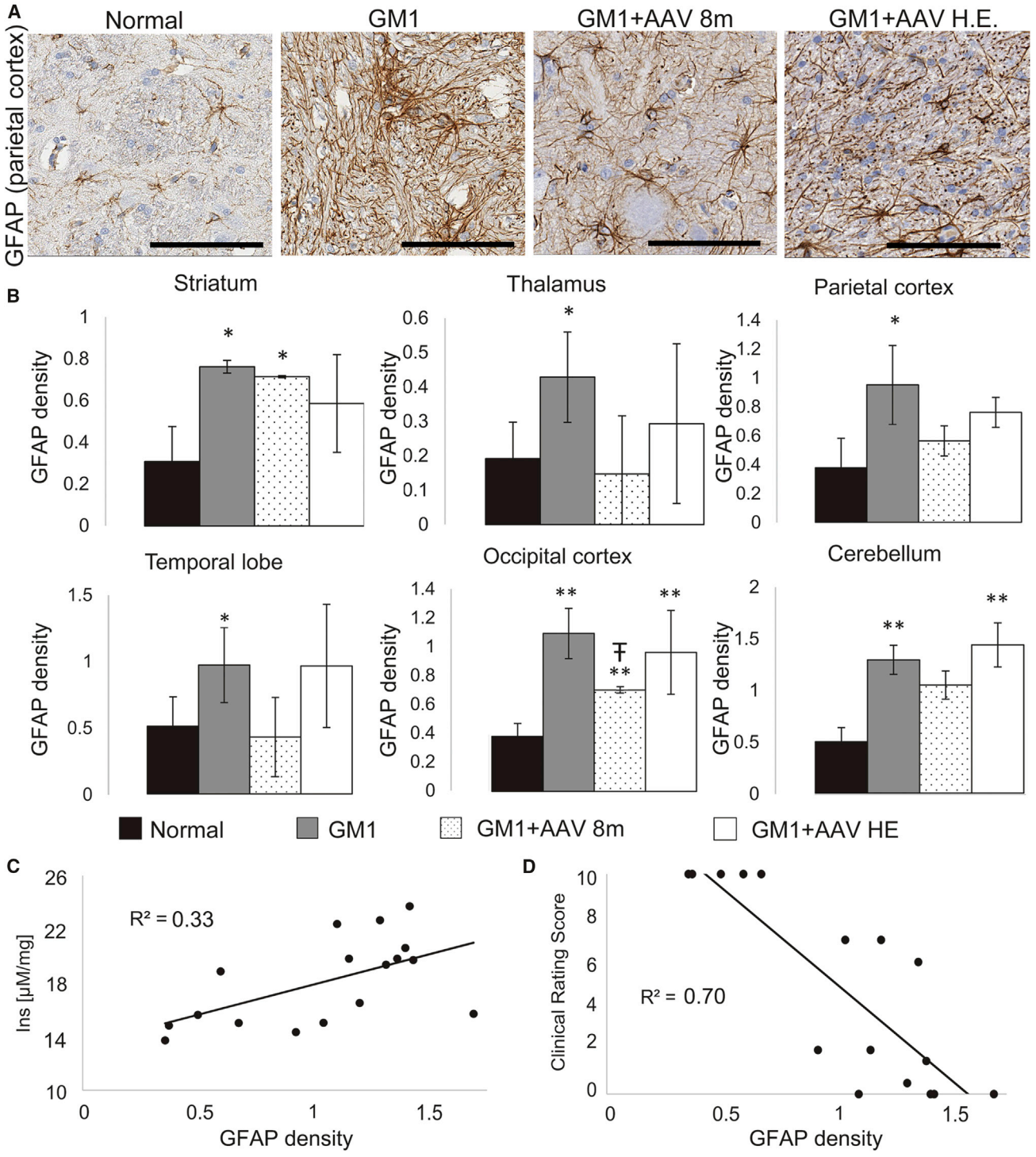

Figure 6. Astrocyte (GFAP) Staining after AAV Gene Therapy (Low Dose)

(A) Representative GFAP staining of the parietal cortex in normal, GM1, or GM1+AAV (low-dose) cats at 8 months and at the humane endpoint. (B) Quantification of GFAP staining in the striatum, thalamus, parietal cortex, temporal lobe, occipital cortex, and cerebellum. (C) Correlation of cerebellar GFAP staining with myoinositol (Ins) concentrations from MRS. (D) Correlation of GFAP staining in the cerebellum with the clinical rating score of cats. *$p < 0.05$, **$p < 0.01$ from age-matched normal controls; $^{\dagger}p < 0.05$, $^{\mp}p < 0.01$ from GM1 cats at the humane endpoint. Error bars represent standard deviation.

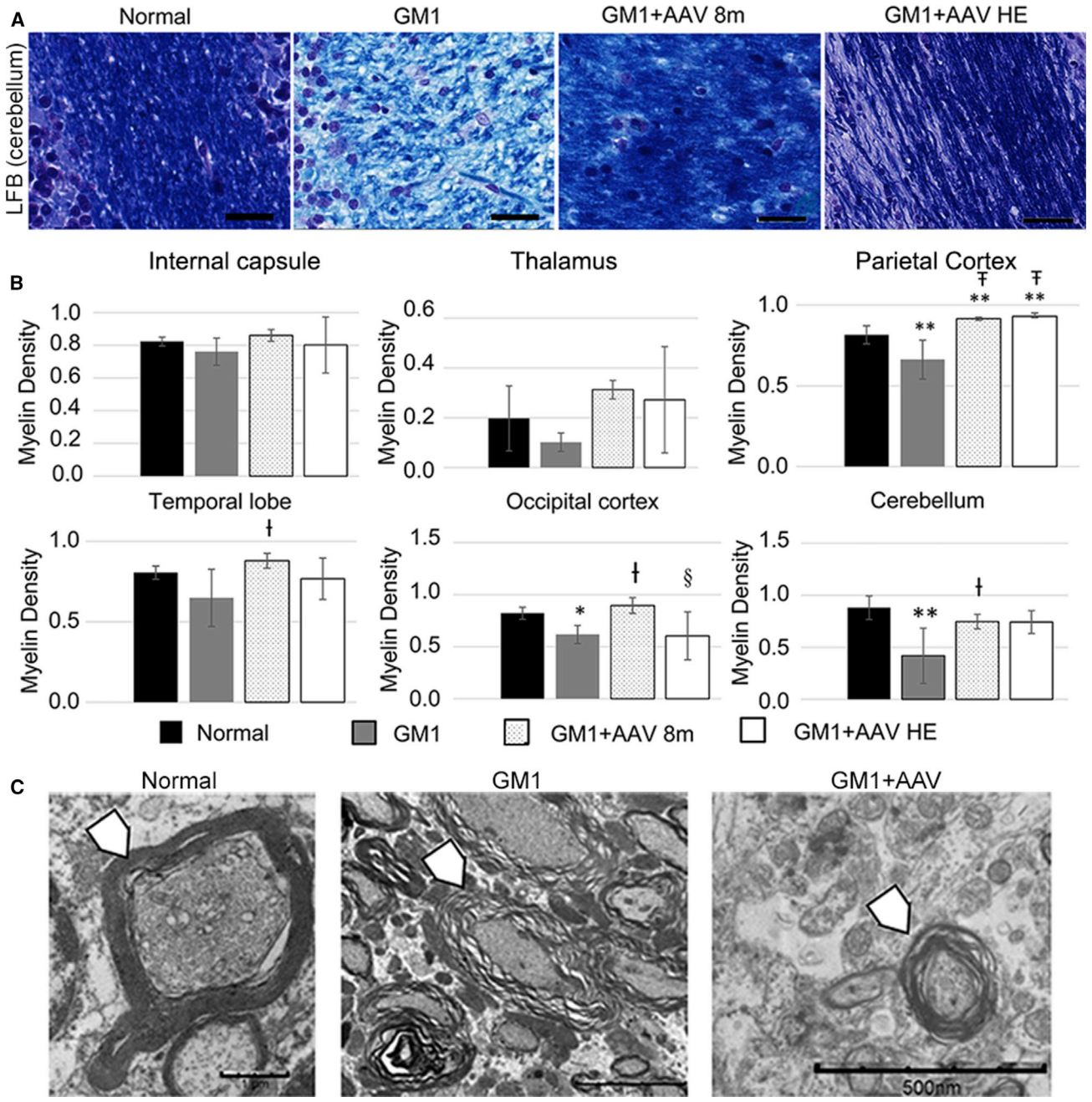

Figure 7. Myelin (Luxol Fast Blue) Staining and the Effect of AAV Gene Therapy

(A) Representative Luxol fast blue stains from normal, GM1, and GM1+AAV (low dose) cats at 8 months and at the humane endpoint (scale bars, 10 μm). (B) Myelin density in the internal capsule, thalamus, parietal cortex, temporal lobe, occipital cortex, and cerebellum. (C) Transmission electronic microscopy (TEM) of the white matter of the temporal lobe of normal (left), untreated GM1 (middle), and GM1+AAV at the humane endpoint (right). White arrows show the myelin sheath. *$p < 0.05$ or **$p < 0.01$ from age-matched normal; $^{\dagger}p < 0.05$ or $^{\text{Ŧ}}p < 0.01$ from GM1 cats at endpoint; $^{\S}p < 0.05$ from 8-month time point. Error bars represent standard deviation.

therapy, neuronal morphology was improved in the parietal cortex, thalamus, and cerebellum, but correction was not achieved in the ventral hippocampus, an area previously shown to be ineffectively treated by Thal injection.[20,26] In GM1+AAV cats at the humane endpoint, Thal and parietal cortex morphology remained partially corrected, whereas neurodegeneration persisted in the cerebellum. White matter was normalized at both 8 months and humane endpoint in treated GM1 cats, in agreement with assessments by MRI.

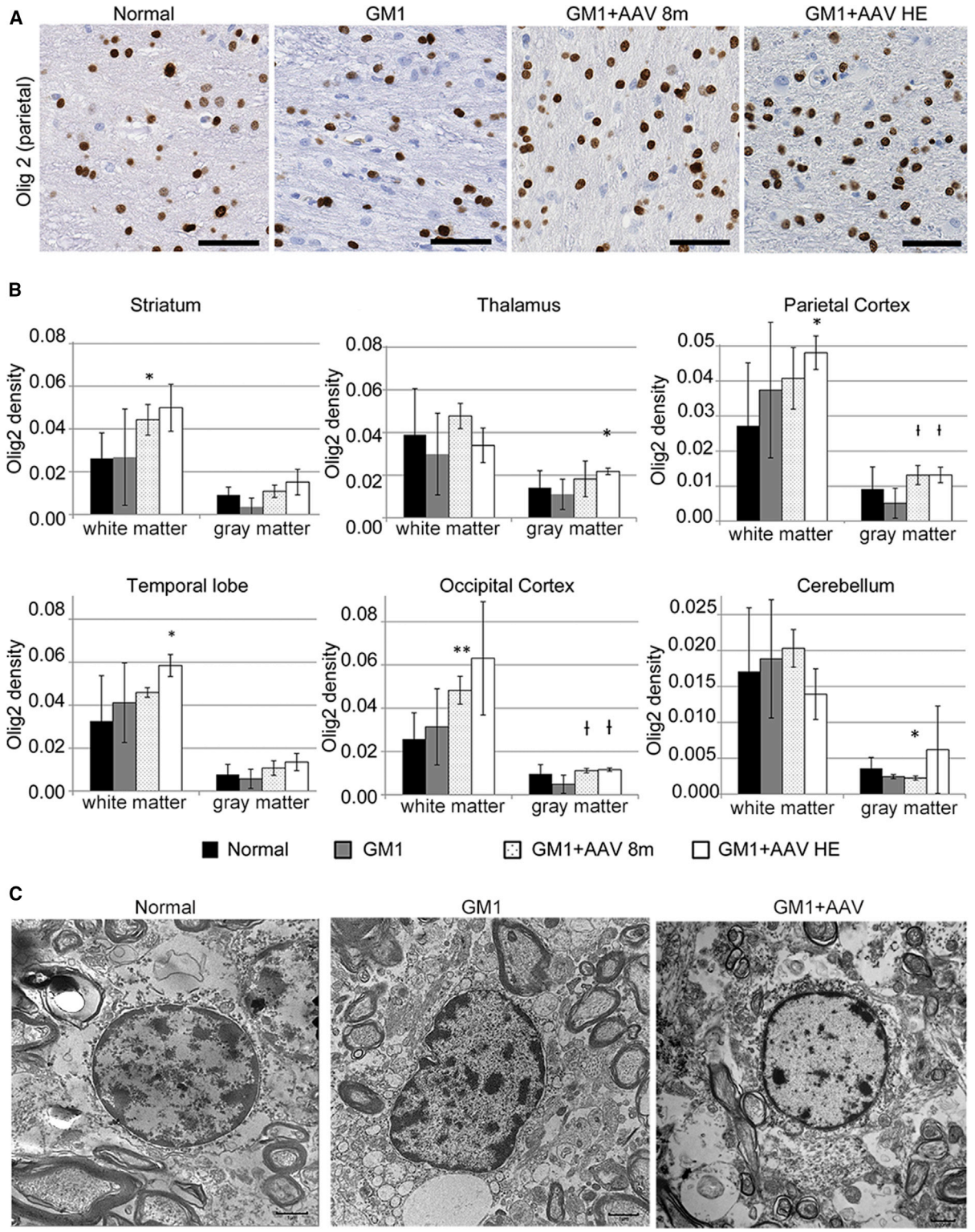

(legend on next page)

Demyelination

Luxol fast blue (LFB) staining for myelin was reduced in untreated GM1 animals in most brain areas with the exception of the internal capsule of the striatum (Figure 7). After AAV gene therapy, myelination was at least partially preserved in all brain areas, both at 8 months and at the humane endpoint. Electron microscopy of myelinated axons in the temporal lobe showed extensive unravelling of myelin in the untreated GM1 cat compared with normal, correlating with previous reports.[19,31] At the humane endpoint, myelination in GM1+AAV cats exhibited a minimal degree of sheath separation and splitting, which was not fully normal but was a clear improvement over untreated GM1 cats.

Oligodendrocytes were evaluated and quantified (Olig2 stain; Figure 8) in an effort to elucidate the mechanism of myelin preservation. In untreated GM1 cats, oligodendrocyte number did not change significantly compared with normal cats, but after AAV gene therapy, oligodendrocyte number increased above normal in many brain areas in both the gray and white matter. Oligodendrocytes from untreated GM1 cats had ultrastructural features of irreversible cell injury, including variation in nuclear shape, undulation of the nuclear envelope, mitochondrial swelling with cristolysis, and swelling/dilatation of the cytocavitary network (Figure 8C). After gene therapy, oligodendrocytes maintained nuclear morphology consistent with what is observed in normal age-matched cats. In addition, oligodendrocytes had a scant amount of electron-dense cytoplasm and appeared to myelinate neuronal processes (data not shown).

DISCUSSION

AAV gene therapy via Thal and DCN injection in GM1 cats has shown profound efficacy resulting in a greater than 7.5-fold increase in lifespan, with four of nine treated cats living beyond 7 years of age and having dramatic improvement in neurologic signs.[20,21] Although very efficacious, direct injection of the cerebellum carries the risk for hemorrhage in the posterior fossa, herniation, and death.

In the current study, i.c.v. injection was tested as an alternative means of treating the cerebellum based on the principle that CSF flows through the ventricular system and into the cisterna magna, thus bathing the cerebellum. Here we tested bilateral Thal injection combined with lateral ventricular infusion at two doses: 5.4×10^{12} vg (n = 1) and 2×10^{12} vg (n = 5). The animal treated with the highest dose has shown substantially improved efficacy and remains alive at 6.5 years of age, similar to survival achieved after combined Thal and DCN delivery (5–8 years of age[20,21]). When GM1 cats treated in the thalamus and DCN were given one-tenth the maximum dose, their survival was extended, but only to 13.9–21.2 months.[20,21] The clear correlation between survival and dose after treatment of the thalamus and DCN also supports the hypothesis that administration of higher doses will lead to improved survival in animals treated by thalamus and i.c.v. injection.

Testing for efficacy at reduced doses is important because application of a lower dose is often tested first in phase I/II clinical trials to show safety prior to dose escalation. This has been well illustrated in a clinical trial for spinal muscular atrophy (ClinicalTrials.gov: NCT02122952), which started with an initial low dose in three patients, then moved to a higher dose with the remaining 12 patients.[32] Although both cohorts received clear benefit from the treatment, the highest dose produced the greatest benefit. Results from the current study show a similar trend and may predict outcomes in future human clinical trials. Also, it is important to test safety and efficacy of different AAV doses in preclinical animal studies before translation to human patients. For example, preclinical studies of AAVrh8 vectors expressing species-matched hexosaminidase, the enzyme missing in Tay-Sachs and Sandhoff diseases, demonstrated toxicity in the brains of nonhuman primates (NHPs).[33] Toxicity was attributed to overexpression of hexosaminidase and did not occur when expression levels were reduced. Multi-year studies using AAV vectors/doses similar to those of the NHP report found no toxicity in wild-type cats or those affected with GM1 or Sandhoff disease.[20,21,25,26,34] Thus, detrimental responses to transgene overexpression, or other aspects of AAV treatment, may be species specific.

We also assessed the ability of ultra-high-field (7T) MRI and MRS to predict pathologic change in discrete brain areas for future clinical trial applications. In line with a previous report,[21] we show a strong correlation between MRI/MRS biomarkers and clinical signs in feline GM1 and also show that MRI-based modalities can be used to infer regional therapeutic efficacy. We report presymptomatic reduction of the neuronal marker NAA and an increase in demyelination markers GPC+PCh. Later MRI and MRS metabolite changes reflect disease progression and amelioration in different brain areas after gene therapy. These results agree with reports from human patients, in which total brain volume and NAA levels highly correlated with disease severity in GM1 patients, further supporting use of MRI and MRS as objective measures in future GM1 clinical trials.[28]

Not surprisingly, the most advanced pathologic changes occurred in brain areas with low β-gal content, demonstrating that correction of neurodegeneration is dependent upon appropriate distribution of therapy to individual brain regions. MRI intensity inversions of gray and white matter reflect the PAS glycolipid profile of the untreated GM1 cat. In AAV-treated cats, brain areas with the highest β-gal activity were normalized on both MRI and PAS staining.

Figure 8. Oligodendrocyte (Olig2) Alterations in GM1 Cats after AAV-Mediated Gene Therapy

(A) Representative photomicrograph of oligodendrocytes in the white matter of normal, GM1, and GM1+AAV-treated cats in the parietal cortex (scale bars, 10 μm). (B) Quantification of oligodendrocyte density in the gray and white matter of the striatum, thalamus, parietal cortex, temporal lobe, occipital cortex, and cerebellum. (C) Transmission electron microscopy (TEM) of oligodendrocytes in the temporal lobe of the normal (left), GM1 (middle), and GM1+AAV cat at the humane endpoint (right). *$p < 0.05$, **$p < 0.01$ from age-matched normal controls; †$p < 0.05$ from GM1 cats at the humane endpoint. Error bars represent standard deviation.

Also, MRS was able to predict histopathologic change in most brain areas. However, it remains unclear why GPC+PCh correlated with myelination in the cerebellum of treated cats at 8 months of age, but not at the humane endpoint. This may represent loss of myelin components not evaluated by LFB staining, because LFB represents staining of lipoproteins. Increased oligodendrocytes (2- to 3-fold) and myelin after AAV gene therapy were noted in areas with β-gal activity above the therapeutic threshold, suggesting that oligodendrocytes can restore myelination through proliferation if sufficient β-gal is present. It remains to be seen whether such remyelination can reverse functional deficits in GM1 patients treated after symptom onset.

Reduction of NAA on MRS reflected neurodegeneration in untreated GM1 cats, but did not reflect normalization of neuronal morphology in the cerebral cortex of treated cats, again at the humane endpoint. We hypothesize this could be because of increased oligodendrocyte number, because NAA is thought to be primarily produced by neurons and used by oligodendrocytes for myelination and as an energy source.[35] This metabolic relationship may indicate why we observed reduced NAA without overt neurodegeneration or neuronal loss. In contrast, evidence of neuronal degeneration was noted in the cerebellum with a concurrent reduction of glutamate. This may indicate loss of glutamatergic neurons, with studies underway to investigate this phenomenon.

Although AAV gene therapy for GM1 administered by Thal and lateral ventricular delivery delayed onset of disease, improved quality of life, and significantly extended lifespan in GM1 cats, the low dose used to treat most animals was suboptimal. This study suggests that high AAV doses are required for effective CSF delivery and should be taken into account in future clinical trial planning.

MATERIALS AND METHODS

Study Objective and Design

The goal of this study was to test the delivery of AAV gene therapy in feline GM1 after Thal and lateral ventricular injection. Cats with GM1 are bred and maintained at Auburn University, and its Institutional Animal Care and Use Committee (IACUC) approved the research described herein. Clinical assessments were made bimonthly on all cats. Clinical rating scores were based on the following clinical signs, with a normal score of 10 and subtraction of one point for each symptom acquired: slight tremors, overt tremors, hindlimb weakness, wide-based stance, ataxia, occasional falling, limited ambulation, spastic front legs, spastic hind legs, and inability to ambulate. GM1 cats were treated at 2–3 months of age with either "high" (5.4×10^{12} vg/animal) or "low" (2.0×10^{12} vg/animal) doses of an AAVrh8 vector encoding feline β-gal. Approximately 20% of the total dose was injected into each thalamus, and the remaining ~60% of the dose was injected into the lateral ventricle as follows. A total of 70 μL was injected into each thalamus in 10- to 20-μL boluses. Injection rate was 2 μL/min, and the needle was raised 0.15 cm between boluses. A total of 200 μL was injected into the left lateral ventricle at a rate of 15 μL/min. AAV vector transgene expression is controlled by a hybrid cytomegalovirus (CMV) enhancer/chicken β-actin promoter and a woodchuck hepatitis virus posttranscriptional regulatory element (WPRE) as previously described.[20,21]

MRI and MRS

MRI and MRS data were acquired as previously described[21] on a 7T MAGNETOM scanner (Siemens Healthcare, Erlangen, Germany) at 4 and 8 months for untreated GM1 cats (n = 4 and n = 6, respectively); at 4 months, 8 months, and 2–5 years for normal controls (n = 4 per time point); and at 8 months or the humane endpoint for the GM1+AAV low-dose group (n = 5). A 32-channel head coil (Nova Medical, Boston, MA, USA) was used for all scans. Anatomical coronal images were acquired using 3D MPRAGE (magnetization-prepared rapid gradient echo) with 0.5-mm isotropic resolution and TR/TE of 1,910/2.5 ms, followed by 2D axial T2 turbo spin echo (TSE) images with TR/TE of 5,450/12 ms and a resolution of $(0.25 \times 0.25 \times 1)$ mm^3. Single-voxel spectroscopy (SVS) was then acquired using PRESS (point resolved spectroscopy) sequence optimized for 7T with TE/TR = 30/5,000 ms, 64 averages, and a variable pulse power and optimized relaxation delays (VAPOR) water suppression. Shimming was performed using FASTESTMAP[36] or a GRE shim sequence (Siemens Healthcare, Erlangen, Germany) followed by manual shimming. The resulting full width at half maximum (FWHM) of the unsuppressed water peak was typically 16 Hz. Optimization of radiofrequency (RF) pulse amplitudes and of the water suppression scheme was performed prior to acquiring each spectrum. The unsuppressed water signal was obtained and used for eddy current correction and for quantification of metabolites. Using high-resolution 3D MRI images, we positioned voxels in the thalamus ($7 \times 6 \times 8$ mm), corona radiata ($7 \times 5 \times 8$ mm), parietal cortex ($7 \times 6 \times 8$ mm), temporal lobe ($7 \times 6 \times 8$mm), occipital cortex ($6 \times 6 \times 5$ mm), and cerebellum ($7 \times 7 \times 8$ mm). MRI data were analyzed with EFilm 3.2 software (Merge Healthcare, Chicago, IL, USA). MRS data were processed with LC model and internal water scaling (http://s-provencher.com/lcmodel.shtml).

Assay of β-Gal Activity

Brain and spinal cord sections were assayed from frozen sections cut from each coronal block. Tissue was homogenized in citrate phosphate buffer (50 mM, pH 4.4) containing 0.1% Triton X-100 and 0.05% bovine serum albumin as previously described.[20] Enzymatic activity was measured using a fluorogenic substrate for β-gal. Specific activity is expressed as nmol 4 MU/mg protein/h as previously described.[20]

Histochemical Staining of β-Gal

For spatial assessment of β-gal activity, frozen sections (40 μm) were thawed and fixed in glutaraldehyde (0.5%) in citrate phosphate buffer (Na2HPO4·7H2O, 50 mM citric acid monohydrate, 10 mM NaCl [pH 4.2 for brain and 5.2 for spinal cord]) for 10 min followed by washes in citrate phosphate buffer. Tissue sections were incubated at 37°C overnight in citrate phosphate buffer (pH 4.2 for brain or pH 5.2 for spinal cord), containing

20 mM $K_4Fe(CN)_6$, 20 mM $K_3Fe(CN)_6$, 2 mM $MgCl_2$, 0.02% Igepal, 0.01% deoxycholic acid, and X-gal (2 mg/mL). The next day, sections were washed, dehydrated, and mounted as previously described.[20]

Immunohistochemistry and Histochemical Staining

LFB staining was performed as previously described.[37] Iba1 (CP290A; Biocare Medical) staining was performed using a 1:100 dilution and overnight incubation as previously described.[38] All other immunohistochemical stains were performed using a Dako automated immunostainer (Autostainer Link48; Dako-Agilent, Santa Clara, CA, USA) using a low pH (6.1) antigen retrieval. Olig2 (EPR2678, 1:200 dilution; Abcam) was incubated for 30 min, and GFAP (IR 52461-2; no dilution; Dako-Agilent, Santa Clara, CA, USA) was incubated for 20 min. Detection was performed using the Dako EnVision HRP detection with DAB chromogen and hematoxylin counterstain. For quantification, slides were digitally scanned at ×80 using an Aperio Scan Scope (Leica Biosystems, Buffalo Grove, IL, USA). Algorithms were written to quantify area of diaminobenzidine (DAB) for each individual stain using Visiopharm quantitative digital histopathology software (Visiopharm, Hoersholm Denmark) and applied to all slides of an individual stain.

PAS Staining for Storage Assessment

The oligosaccharide side chain of ganglioside was qualitatively assessed using PAS staining. Frozen sections (40 μm) were washed in phosphate-buffered saline (PBS), fixed for 7 min with 3.7% paraformaldehyde in 95% ethanol/5% double-distilled water (ddH_2O) (pH 7.4), washed again with PBS, incubated for 3 min in 0.5% periodic acid, washed in ddH_2O, and incubated in Schiff reagent for 45 (brain) or 60 s (spinal cord) as previously described.[20]

qPCR for AAV Biodistribution

Vector was measured by qPCR with SYBR green-based reactions (Bio-Rad, Hercules, CA, USA) with primers specific for WPRE in the vector (forward, 5′-AGTTGTGGCCCGTTGTCA-3′; reverse, 5′-GAGGGGGAAAGCGAAAGT-3′). Cycle parameters were as follows: 95°C for 10 min followed by 40 cycles of 95°C for 15 s and 60°C for 1 min. Genomic DNA samples (50 ng/sample) were measured in duplicate using a Bio-Rad CFX96 Real-Time System and compared with a standard curve of a plasmid containing the WPRE sequence as previously described.[20]

Statistics

Statistical analyses were performed using Microsoft Excel (Microsoft, Redmond, WA, USA) and Prism (GraphPad, San Diego, CA, USA). Two-sided, paired Student's t test assuming unequal variances was utilized for statistical comparisons between groups. p values are indicated from normal (*$p < 0.05$, **$p < 0.01$) and untreated GM1 cats ($^{\dagger}p < 0.05$, $^{\mp}p < 0.01$). For MRS, only spectra with a Cramér-Rao minimum variance bounds of <30 were included in analysis. Regression analyses (R^2) were used to correlate clinical signs with metabolite concentrations.

SUPPLEMENTAL INFORMATION

Supplemental Information can be found online at https://doi.org/10.1016/j.omtm.2019.11.023.

AUTHOR CONTRIBUTIONS

Conceptualization, H.L.G.-E., M.S.-E., and D.R.M.; Methodology, H.L.G.-E., A.S.M., N.S., A.N.R., T.S.D., R.J.B., A.S.G., A.R.B., M.S.-E., and D.R.M.; Investigation, H.L.G.-E., A.S.M., L.E.E., T.L.V., E.B.D., J.K., A.R.T., B.L.B., and A.L.G.; Writing – Original Draft, H.L.G.-E.; Writing – Review & Editing, M.S.-E. and D.R.M.; Funding Acquisition, H.L.G.-E., T.S.D., M.S.-E., and D.R.M.; Resources, T.S.D., M.S.-E., and D.R.M.; Visualization, H.L.G.-E., A.S.M., B.L.B., and D.R.M.; Supervision, N.S., T.S.D., M.S.-E., and D.R.M.

ACKNOWLEDGMENTS

This work was funded by NIH grants F32 NS080488 (to H.L.G.-E.) and R01 HD060576 (to M.S.-E. and D.R.M.). H.L.G.-E., M.S.-E., and D.R.M. are beneficiaries of a licensing agreement with Axovant Gene Therapies (New York, NY, USA) based partly on this technology. M.S.-E. and D.R.M. are shareholders in Lysogene (Neuilly-sur-Seine, France).

REFERENCES

1. Regier, D.S., and Tifft, C.J. (2013). GLB1-related disorders. In GeneReviews, R.A. Pagon, M.P. Adam, H.H. Ardinger, S.E. Wallace, A. Amemiya, and L.J.H. Bean, et al., eds. (University of Washington).
2. Suzuki, Y., Sakuraba, H., and Oshima, A. (1995). Beta-galactosidase deficiency (beta-galactosidosis): GM1 gangliosidosis and Morquio B disease. In The Metabolic and Molecular Bases of Inherited Disease, Seventh Edition, *Volume 2*, C.R. Scriver, A.L. Beaudet, W.S. Sly, and D. Valle, eds (McGraw-Hill, Inc.), pp. 2785–2823.
3. Rama Rao, K.V., and Kielian, T. (2016). Astrocytes and lysosomal storage diseases. Neuroscience *323*, 195–206.
4. van der Voorn, J.P., Kamphorst, W., van der Knaap, M.S., and Powers, J.M. (2004). The leukoencephalopathy of infantile GM1 gangliosidosis: oligodendrocytic loss and axonal dysfunction. Acta Neuropathol. *107*, 539–545.
5. Imamura, A., Miyajima, H., Ito, R., and Orii, K.O. (2008). Serial MR imaging and 1H-MR spectroscopy in monozygotic twins with Tay-Sachs disease. Neuropediatrics *39*, 259–263.
6. Aydin, K., Bakir, B., Tatli, B., Terzibasioglu, E., and Ozmen, M. (2005). Proton MR spectroscopy in three children with Tay-Sachs disease. Pediatr. Radiol. *35*, 1081–1085.
7. Wilken, B., Dechent, P., Hanefeld, F., and Frahm, J. (2008). Proton MRS of a child with Sandhoff disease reveals elevated brain hexosamine. Eur. J. Paediatr. Neurol. *12*, 56–60.
8. Miller, B.L. (1991). A review of chemical issues in 1H NMR spectroscopy: N-acetyl-L-aspartate, creatine and choline. NMR Biomed. *4*, 47–52.
9. Assadi, M., Baseman, S., Janson, C., Wang, D.J., Bilaniuk, L., and Leone, P. (2008). Serial 1H-MRS in GM2 gangliosidoses. Eur. J. Pediatr. *167*, 347–352.
10. Brunetti-Pierri, N., Bhattacharjee, M.B., Wang, Z.J., Zili Chu, Wenger, D.A., Potocki, L., Hunter, J., and Scaglia, F. (2008). Brain proton magnetic resonance spectroscopy and neuromuscular pathology in a patient with GM1 gangliosidosis. J. Child Neurol. *23*, 73–78.
11. De Grandis, E., Di Rocco, M., Pessagno, A., Veneselli, E., and Rossi, A. (2009). MR imaging findings in 2 cases of late infantile GM1 gangliosidosis. AJNR Am. J. Neuroradiol. *30*, 1325–1327.
12. Erol, I., Alehan, F., Pourbagher, M.A., Canan, O., and Vefa Yildirim, S. (2006). Neuroimaging findings in infantile GM1 gangliosidosis. Eur. J. Paediatr. Neurol. *10*, 245–248.

13. Hasegawa, D., Yamato, O., Nakamoto, Y., Ozawa, T., Yabuki, A., Itamoto, K., Kuwabara, T., Fujita, M., Takahashi, K., Mizoguchi, S., and Orima, H. (2012). Serial MRI features of canine GM1 gangliosidosis: a possible imaging biomarker for diagnosis and progression of the disease. ScientificWorldJournal *2012*, 250197.

14. Kaye, E.M., Alroy, J., Raghavan, S.S., Schwarting, G.A., Adelman, L.S., Runge, V., Gelblum, D., Thalhammer, J.G., and Zuniga, G. (1992). Dysmyelinogenesis in animal model of GM1 gangliosidosis. Pediatr. Neurol. *8*, 255–261.

15. Bitsch, A., Bruhn, H., Vougioukas, V., Stringaris, A., Lassmann, H., Frahm, J., and Brück, W. (1999). Inflammatory CNS demyelination: histopathologic correlation with in vivo quantitative proton MR spectroscopy. AJNR Am. J. Neuroradiol. *20*, 1619–1627.

16. Ul Haque, A. (1995). Fine needle aspiration cytology of Tay-Sachs disease. A case report. Acta Cytol. *39*, 762–765.

17. Moriwaki, S., Takashima, S., Yoshida, H., Kawano, N., and Goto, M. (1977). Histological observation of the brain of Tay-Sachs disease with seizure and chronic DPH intoxication—report of an autopsy case. Acta Pathol. Jpn. *27*, 387–407.

18. Brand, A., Richter-Landsberg, C., and Leibfritz, D. (1993). Multinuclear NMR studies on the energy metabolism of glial and neuronal cells. Dev. Neurosci. *15*, 289–298.

19. Baker, H.J., Jr., Lindsey, J.R., McKhann, G.M., and Farrell, D.F. (1971). Neuronal GM1 gangliosidosis in a Siamese cat with beta-galactosidase deficiency. Science *174*, 838–839.

20. McCurdy, V.J., Johnson, A.K., Gray-Edwards, H.L., Randle, A.N., Brunson, B.L., Morrison, N.E., Salibi, N., Johnson, J.A., Hwang, M., Beyers, R.J., et al. (2014). Sustained normalization of neurological disease after intracranial gene therapy in a feline model. Sci. Transl. Med. *6*, 231ra48.

21. Gray-Edwards, H.L., Regier, D.S., Shirley, J.L., Randle, A.N., Salibi, N., Thomas, S.E., Latour, Y.L., Johnston, J., Golas, G., Maguire, A.S., et al. (2017). Novel Biomarkers of Human GM1 Gangliosidosis Reflect the Clinical Efficacy of Gene Therapy in a Feline Model. Mol. Ther. *25*, 892–903.

22. Broekman, M.L., Baek, R.C., Comer, L.A., Fernandez, J.L., Seyfried, T.N., and Sena-Esteves, M. (2007). Complete correction of enzymatic deficiency and neurochemistry in the GM1-gangliosidosis mouse brain by neonatal adeno-associated virus-mediated gene delivery. Mol. Ther. *15*, 30–37.

23. Weismann, C.M., Ferreira, J., Keeler, A.M., Su, Q., Qui, L., Shaffer, S.A., Xu, Z., Gao, G., and Sena-Esteves, M. (2015). Systemic AAV9 gene transfer in adult GM1 gangliosidosis mice reduces lysosomal storage in CNS and extends lifespan. Hum. Mol. Genet. *24*, 4353–4364.

24. Baek, R.C., Broekman, M.L., Leroy, S.G., Tierney, L.A., Sandberg, M.A., d'Azzo, A., Seyfried, T.N., and Sena-Esteves, M. (2010). AAV-mediated gene delivery in adult GM1-gangliosidosis mice corrects lysosomal storage in CNS and improves survival. PLoS ONE *5*, e13468.

25. Rockwell, H.E., McCurdy, V.J., Eaton, S.C., Wilson, D.U., Johnson, A.K., Randle, A.N., Bradbury, A.M., Gray-Edwards, H.L., Baker, H.J., Hudson, J.A., et al. (2015). AAV-mediated gene delivery in a feline model of Sandhoff disease corrects lysosomal storage in the central nervous system. ASN Neuro. *7*, 1759091415569908.

26. McCurdy, V.J., Rockwell, H.E., Arthur, J.R., Bradbury, A.M., Johnson, A.K., Randle, A.N., Brunson, B.L., Hwang, M., Gray-Edwards, H.L., Morrison, N.E., et al. (2015). Widespread correction of central nervous system disease after intracranial gene therapy in a feline model of Sandhoff disease. Gene Ther. *22*, 181–189.

27. Ellinwood, N.M., Vite, C.H., and Haskins, M.E. (2004). Gene therapy for lysosomal storage diseases: the lessons and promise of animal models. J. Gene Med. *6*, 481–506.

28. Regier, D.S., Kwon, H.J., Johnston, J., Golas, G., Yang, S., Wiggs, E., Latour, Y., Thomas, S., Portner, C., Adams, D., et al. (2016). MRI/MRS as a surrogate marker for clinical progression in GM1 gangliosidosis. Am. J. Med. Genet. A. *170*, 634–644.

29. Conzelmann, E., and Sandhoff, K. (1983-1984). Partial enzyme deficiencies: residual activities and the development of neurological disorders. Dev. Neurosci. *6*, 58–71.

30. Navon, R., Padeh, B., and Adam, A. (1973). Apparent deficiency of hexosaminidase A in healthy members of a family with Tay-Sachs disease. Am. J. Hum. Genet. *25*, 287–293.

31. Baker, H.J., Reynolds, G.D., Walkley, S.U., Cox, N.R., and Baker, G.H. (1979). The gangliosidoses: comparative features and research applications. Vet. Pathol. *16*, 635–649.

32. Mendell, J.R., Al-Zaidy, S., Shell, R., Arnold, W.D., Rodino-Klapac, L.R., Prior, T.W., Lowes, L., Alfano, L., Berry, K., Church, K., et al. (2017). Single-Dose Gene-Replacement Therapy for Spinal Muscular Atrophy. N. Engl. J. Med. *377*, 1713–1722.

33. Golebiowski, D., van der Bom, I.M.J., Kwon, C.S., Miller, A.D., Petrosky, K., Bradbury, A.M., Maitland, S., Kühn, A.L., Bishop, N., Curran, E., et al. (2017). Direct Intracranial Injection of AAVrh8 Encoding Monkey β-N-Acetylhexosaminidase Causes Neurotoxicity in the Primate Brain. Hum. Gene Ther. *28*, 510–522.

34. Bradbury, A.M., Cochran, J.N., McCurdy, V.J., Johnson, A.K., Brunson, B.L., Gray-Edwards, H., Leroy, S.G., Hwang, M., Randle, A.N., Jackson, L.S., et al. (2013). Therapeutic response in feline sandhoff disease despite immunity to intracranial gene therapy. Mol. Ther. *21*, 1306–1315.

35. Moffett, J.R., Arun, P., Ariyannur, P.S., and Namboodiri, A.M. (2013). N-Acetylaspartate reductions in brain injury: impact on post-injury neuroenergetics, lipid synthesis, and protein acetylation. Front. Neuroenergetics *5*, 11.

36. Gruetter, R., and Tkác, I. (2000). Field mapping without reference scan using asymmetric echo-planar techniques. Magn. Reson. Med. *43*, 319–323.

37. Luna, L.G. (1968). Manual of Histologic Staining Methods of the Armed Forces Institute of Pathology. In Methods for Nerve Cells and Fibers, Third Edition (McGraw-Hill), pp. 203–204.

38. Bradbury, A.M., Peterson, T.A., Gross, A.L., Wells, S.Z., McCurdy, V.J., Wolfe, K.G., Dennis, J.C., Brunson, B.L., Gray-Edwards, H., Randle, A.N., et al. (2017). AAV-mediated gene delivery attenuates neuroinflammation in feline Sandhoff disease. Neuroscience *340*, 117–125.